Journal of Catalysis **182,** 479–488 (1999)
Article ID jcat.1998.2364, available online at http://www.idealibrary.com on IDEAL®

Nitrogen Adsorption and Dissociation on Fe(111)

J. J. Mortensen,* L. B. Hansen,* B. Hammer,*,† and J. K. Nørskov*

*Center for Atomic-Scale Materials Physics, Department of Physics, Technical University of Denmark, DK-2800 Lyngby, Denmark; and †Institute of Physics, Aalborg University, Pontoppidanstræde 103, DK-9220 Aalborg Ø, Denmark

Received August 20, 1998; revised November 16, 1998; accepted November 17, 1998

We report extensive density functional calculations of the energetics of N_2 adsorption and dissociation on a Fe(111) surface. From the calculations we can present a detailed picture of the rate limiting step in the ammonia synthesis which is consistent with available experimental observations. Four different molecularly adsorbed states are identified, including a new state not seen by experiment. The new state is the true precursor to dissociation. We find that there are two dissociation channels, one going through all the molecular states sequentially with a low energy barrier, but a high entropy barrier, and the other a direct channel into the new precursor, which is highly activated. In this way we can explain both the measured sticking probability for a thermal gas of N_2 above a Fe(111) surface and the molecular beam scattering experiments. During ammonia synthesis conditions the low barrier channel is expected to dominate, but at the highest synthesis temperatures, the high barrier channels may become the most effective. The origin of the alkali promotion of the N_2 dissociation process is also discussed. © 1999 Academic Press

1. INTRODUCTION

The synthesis of ammonia from nitrogen and hydrogen takes place industrially over an iron-based catalyst. This was the first large scale industrial catalyst system, developed by Haber and Bosch at the beginning of this century (1), and since its discovery it has been studied extensively (2–9). Many of the elementary processes have been described in detail, and when combined with a microkinetic model of the synthesis rate, the measured N_2 dissociation and desorption rates (7) can be transformed into a prediction of the ammonia synthesis rate at industrial conditions (100 atm and 700 K), which is within a factor of two of the measured one (10–12).

It is generally agreed that the dissociation of the N_2 molecule is the rate limiting step in the reaction, but there is not an atomistic mechanism for this reaction which can explain all the experimental observations. One fundamental, unanswered question is why some experiments show the dissociation of N_2 to be nonactivated (1, 7, 8, 13), while others show it to be strongly activated (14). Other open questions are why the dissociation probability for N_2 is as low as 10^{-5} even on the most reactive Fe(111) surface (7, 8), and what the nature of the active site is.

In the present paper we contribute to a settlement of these questions by a set of detailed density functional theory (DFT) calculations of the adsorption and dissociation of N_2 on Fe(111). Based on the calculations, we present a detailed picture of the dissociation process which is consistent with all available experimental observations. The key to the understanding is the finding of a new molecular precursor to dissociation, which can be accessed either through a zero activation energy channel with a high entropic barrier or through a high activation energy channel with a low entropic barrier.

In the following we first describe in some detail the experimental situation. We also give a short treatment of transition state theory, which is needed in order to relate calculated activation energies to reaction rates. We then describe the calculation method and continue with a detailed treatment of the atomically adsorbed state, the surface diffusion of adsorbed nitrogen, the molecularly adsorbed states, and finally the dissociation process. Along the way we discuss the relation of the calculated results to experiment.

2. SUMMARY OF EXPERIMENTAL RESULTS

A large number of very detailed experiments have been aimed at understanding the adsorption and dissociation of N_2 on single crystal iron surfaces, in particular the (111) surface, which is the most reactive. In the following we first consider results obtained from experiments where a gas of N_2 molecules at a specified temperature is adsorbed on a Fe(111) surface.

Figure 1 shows the established potential energy diagram for N_2 adsorption and dissociation on Fe(111). There are two weakly adsorbed molecular states γ and α with desorption temperatures of 98 and 160 K, respectively (15, 17). The sticking probability into the γ state is $\sigma_\gamma \geq 0.7$ (18), which is the usual order of magnitude for molecular adsorption. The sticking probability into the α state is $\sigma_\alpha = 10^{-2\pm0.5}$ (15). As indicated in Fig. 1 adsorption into the

0021-9517/99 $30.00

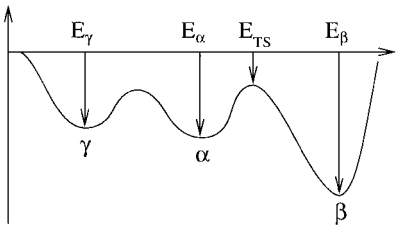

FIG. 1. Schematic potential energy surface for N_2 adsorption and dissociation above a Fe(111) surface deduced from experiment. Two molecularly adsorbed states, γ and α, and the dissociated state, β, are shown. The energy is not drawn to scale. The energies shown in the figure, $E_\gamma \simeq -0.3$ eV/molecule, $E_\alpha = -0.33$ eV/molecule, $E_\beta = -2.2$ eV/molecule, and $E_{TS} = -0.034$ eV, are experimental values taken from Refs. (17), (15), (15), and (15), respectively.

α state can take place via the γ state (17, 18). At higher temperatures a direct channel from the gas phase into the α state is known to be important (17).

Dissociation is known to proceed via the α state with an overall initial sticking probability of the order $\sigma_\beta \sim 10^{-5}$ (β is the conventional notation for adsorbed atomic N). Ertl *et al.* (15) measured σ_β in the temperature range between 214 and 423 K and found a slight decrease in the initial sticking probability with increasing temperature. It is parameterized as (15)

$$\sigma_\beta = \nu_\sigma \exp(-E_{TS}/kT), \quad \nu_\sigma = 2.2 \times 10^{-6}, \quad E_{TS} = -0.034 \text{ eV}. \qquad [1]$$

A negative value for E_{TS} suggests that the top of the barrier for the transition from α to β is below the energy of the molecule in the gas phase (see Fig. 1).

The γ state is oriented perpendicular to the surface and the α state adsorbs in a configuration where both N atoms interact with the surface (19). The γ and α states have saturation coverages of ~0.5 and ~0.1 ML (18).

Another important fingerprint that can be used to identify the different molecular states is the measured vibrational frequency. The $^{15}N_2$ frequencies are shifted from the gas-phase value of 282 meV to 260 meV for the γ state (20) and to 185 meV for the α state (19).

The results of the experiments using a thermal gas of N_2 above the surface can be contrasted with the results of molecular beam scattering experiments by Rettner and Stein (14). At low kinetic energies σ_β is about 10^{-6}, close to the value found for a thermal gas. Increasing the kinetic energy to 1 eV increases σ_β by more than four orders of magnitude. Increasing the energy further leads to a saturation of σ_β at ~0.1. The simple picture in Fig. 1 cannot explain this behavior, because trapping in the γ or α state will be less efficient at higher incident energies. It was therefore concluded that there is an energy barrier between the gas phase and some adsorbed state from where the molecule can dissociate. It is probably not a direct path from the gas phase to the dissociated state β, because a surface temperature dependence of σ_β for fixed kinetic energy is also observed. An Arrhenius plot of the sticking probability σ_β versus surface temperature gives an activation energy of -0.023 ± 0.006 eV (14), in good agreement with the thermal gas experiments (see Eq. [1]). One possibility is that it is the α state which is accessed via an activated direct path. This is, however, not consistent with the work of Ertl *et al.* (15). From this we know that $\sigma_\alpha \sim 10^{-2}$ and $\sigma_\beta \sim 10^{-5}$, meaning that only 1 out of 10^3 molecules in the α state is dissociating instead of desorbing. Since the probability that a molecule in the beam has access to the α state is at most 1, we should not expect dissociative sticking probabilities above 10^{-3}, which is clearly not in agreement with the observations.

A negative effective activation energy (Eq. [1]) is consistently found in measurements of the temperature dependence of the sticking probability. In Fig. 2 we summarize results from three independent experiments. Apart from the results from Eq. [1], we include in the figure results from Grunze (1) and the most recent from Alstrup *et al.* In the latter work, pressures up to 500 Torr were used, so that the gas temperature is equal to the surface temperature of the sample. It was demonstrated that the initial sticking probability σ_β does not depend on the gas temperature. This is in good agreement with a molecular precursor mechanism, because molecules in the α state will quickly equilibrate with the surface and "forget" their gas temperature.

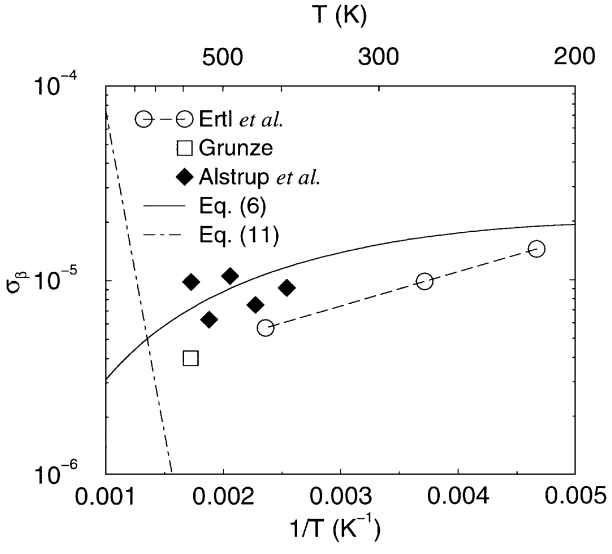

FIG. 2. Arrhenius plot of the initial sticking probability for dissociative adsorption of N_2 of Fe(111). The experimental results are from (1, 13, 15). The full curve is a model calculation for an indirect adsorption via the α state using Eq. [6] with $q_{TS} = 1$ and $E_{TS} = 0.03$ eV. The dashed curve is calculated assuming direct adsorption into the α' state using Eq. [11], with $E^{dir} = 0.64$ eV and $s_0 = 0.17$.

The results in Fig. 2 raise the question of why the dissociation of a molecule in the α state is so much disfavored compared to thermal desorption, when the apparent dissociation barrier is 0.034 eV lower than the desorption barrier.

3. TRANSITION STATE THEORY

Before entering into the results from our DFT calculations, we will briefly show how to calculate σ_β using transition state theory.

We assume that the population of the α state is in equilibrium with the gas phase. If the precursor has a coverage of θ_α, and the rate with which a molecule in the α state dissociates is k, then the rate of dissociation per site will be $\theta_\alpha k$. If the molecule is equilibrated in the α state, one can use transition state theory to estimate

$$k = \frac{kT}{h}\frac{q_{\mathrm{TS}}}{q_\alpha}e^{(E_\alpha - E_{\mathrm{TS}})/kT}, \qquad [2]$$

where q_{TS}, q_α and E_{TS}, E_α are the partition functions and the adsorption energies for the molecule in the transition state and in the α state, respectively. Here and throughout we define the adsorption energy relative to the energy of the clean surface and the gas phase N_2 molecule as

$$E_x = E(x - \mathrm{N_2/Fe}) - E(\mathrm{Fe}) - E(\mathrm{N_2}), \qquad [3]$$

where x denotes the adsorption state of the molecule. The degree of freedom of the reaction coordinate should be excluded in the calculation of q_{TS} and the zero point energy of this coordinate should not be included in E_{TS} either. From q_α and the partition function for a gas molecule, q_{gas}, we can calculate the coverage, θ_α, of the α state in equilibrium with the gas phase. Since $|E_\alpha|$ is small we can assume $\theta_\alpha \ll 1$ at room temperature and above. In this case we have

$$\theta_\alpha = \frac{q_\alpha}{q_{\mathrm{gas}}}e^{-E_\alpha/kT}. \qquad [4]$$

At any reasonable temperatures the N–N vibrations are frozen out, and only rotations and translation will contribute to the partition function for a gas molecule; its partition function can be written

$$q_{\mathrm{gas}} = \frac{kT}{2\varepsilon_{\mathrm{rot}}}\frac{kT}{P}\left(\frac{2\pi mkT}{h^2}\right)^{3/2}, \qquad [5]$$

where P is the gas pressure and $\varepsilon_{\mathrm{rot}} = 0.248$ meV is the rotational constant for N_2 (22).

The sticking probability can now be calculated as $\sigma_\beta = \theta_\alpha k/(FA)$, where $F = P/\sqrt{2\pi mkT}$ is the flux of molecules hitting the surface and $A = \sqrt{3}a^2 = 14.3$ Å^2 is the area per site. Putting everything together we get

$$\sigma_\beta = \frac{1}{FA}\frac{kT}{h}\frac{q_{\mathrm{TS}}}{q_{\mathrm{gas}}}e^{-E_{\mathrm{TS}}/kT} = \frac{\varepsilon_{\mathrm{rot}}h^2 q_{\mathrm{TS}}}{\pi Am(kT)^2}e^{-E_{\mathrm{TS}}/kT}. \qquad [6]$$

Neglecting the substrate degrees of freedom, the partition function for the transition state complex is obtained from the five real normal mode frequencies ω_i (there is a sixth imaginary frequency belonging to the normal mode along the dissociation reaction path)

$$q_{\mathrm{TS}} = \prod_i \frac{1}{1 - e^{-\hbar\omega_i/kT}}. \qquad [7]$$

For now we assume that all $\hbar\omega_i$'s are larger than kT. In this limit we get $q_{\mathrm{TS}} = 1$.

At room temperature the prefactor in Eq. [6] is 0.5×10^{-4}, and with a negative activation energy $E_{\mathrm{TS}} = -0.034$ eV (Eq. [1]) we get a dissociative sticking probability about two orders of magnitude higher than experimentally observed.

The temperature dependence of the prefactor is important, however. In Eq. [1] the value for E_{TS} was fitted to account for the slight decrease in σ_β with increasing temperature, and the prefactor was a constant. The prefactor in Eq. [6] alone gives the observed temperature dependence because the entropy of the gas increases with temperature. If we calculate the Arrhenius slope from Eq. [6] we get the effective activation energy as

$$-\frac{d\ln(\sigma_\beta)}{d(1/kT)} = E_{\mathrm{TS}} - 2kT. \qquad [8]$$

This equation shows that we can choose E_{TS} slightly *positive* and still get a negative effective activation energy. With $E_{\mathrm{TS}} = 0.03$ eV we get the full line in Fig. 2. We see that this result describes reasonably well all the measured data.

4. THE DFT CALCULATIONS

In the DFT calculations, we model the surface by a periodic array of (111) oriented slabs. The slabs consist of six layers of Fe atoms, which corresponds to a thickness of approximately 7 Å. The total height of the unit cell is 15 Å. Top and side views of the slab are shown in Fig. 3. Two different surface unit cells are used, a (1×1) and a $(\sqrt{3} \times \sqrt{3})\mathrm{R}30^\circ$ cell corresponding to a coverage of 1 or 1/3, respectively. The latter cell is the largest we can handle computationally, but due to the very open structure of the bcc(111) surface, the distance between adsorbates is very large, and interactions from one unit cell to the next should be small.

The Kohn–Sham equations are solved by expanding the wavefunctions in plane waves (23). Ultrasoft pseudopotentials are used to describe the ion cores (24) and plane waves with a kinetic energy up to 25 Ry are included. The **k**-points used are chosen so that equivalent sampling of the Brillouin zones (BZ) for different surface unit cells is ensured. For a discussion of convergence of the results with respect to the number of layers and **k**-points we refer to Ref. (25), where the atomic adsorption of N on Fe(111) is treated in

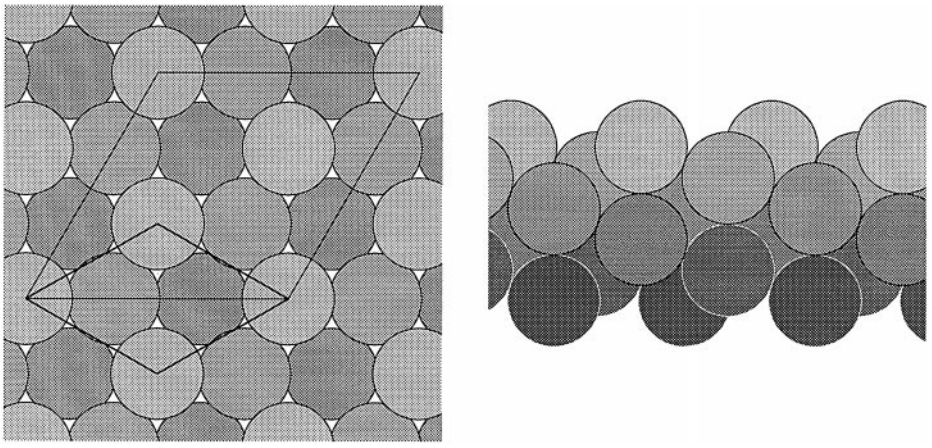

FIG. 3. Top and side views of the clean six layer Fe(111) slab used to model the Fe(111) surface. Both the (1×1) and the $(\sqrt{3} \times \sqrt{3})$R30° cells used in the calculations are shown. The first three layers of the slab are allowed to relax.

detail. We have found that 54 **k**-points in the first BZ (18 for the $(\sqrt{3} \times \sqrt{3})$R30° cell) and 6 layers of Fe give sufficient accuracy for the calculation of adsorption energies.

All calculations are fully spin polarized, and the self-consistent solutions of the Kohn–Sham equations and geometry optimizations are done using the PW91 exchange correlation energy (26). The total energies are then calculated from the PW91 electron densities using the more accurate PBE functional (27) with $\kappa = 1.245$ (28, 29). While the absolute values of the adsorption energies depend on the choice of exchange-correlation functional the relative energies and all qualitative results are independent of this choice.

5. ADSORBED STATES

We have found five local minima for N_2 on Fe(111). Four of them are molecularly adsorbed states while the fifth is the atomically adsorbed β state. In the following we first consider the atomically adsorbed state and then the molecularly adsorbed states, one by one.

5.1. Atomic N on Fe Single Crystal Surfaces

The adsorption of atomic N on Fe(111) and the other low index Fe surfaces has been discussed in detail in Ref. (25). Here we just summarize the results of particular importance in connection with an understanding of the dissociation process.

The calculated equilibrium site for a simple (1×1) overlayer structure of N atoms on Fe(111) is illustrated in Fig. 4. The adsorption energy as a function of coverage for all three low index Fe surfaces is shown in Fig. 5.

On the unreconstructed Fe(111) surface the calculated adsorption energy of atomic N is –1.4 eV/molecule. On Fe(100), on the other hand, N binds much more strongly (–2.4 eV/molecule) in a c(2×2) structure at 1/2 ML coverage (25). On the Fe(100) surface this is the experimentally observed structure (21), and the calculated adsorption energy agrees well with experiment (13, 15). Atomic nitrogen adsorbed on the Fe(111) surface is known to form ordered structures with large unit cells and with a binding energy which is only slightly smaller than on Fe(100) (13, 15).

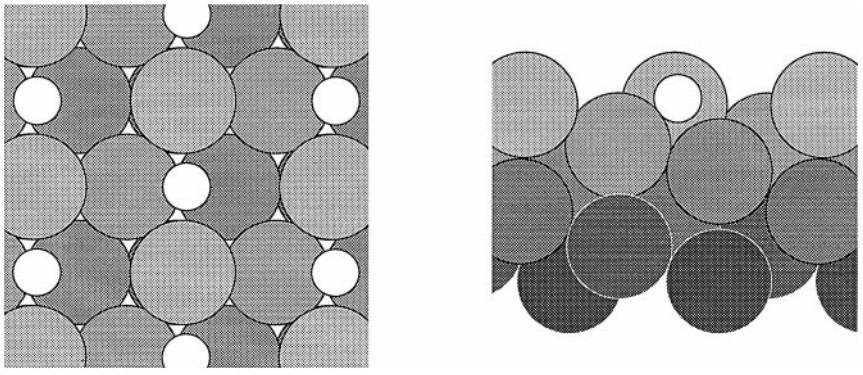

FIG. 4. Top and side views of N adsorbed on Fe(111)

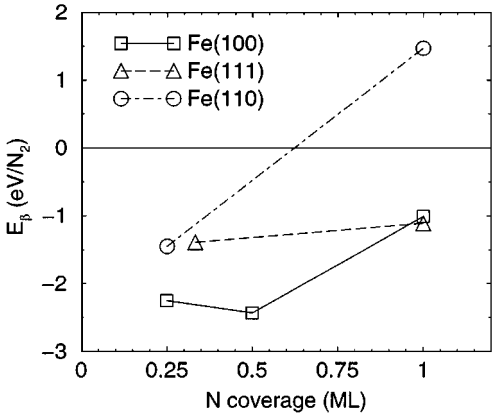

FIG. 5. Adsorption energies for N on Fe as a function of coverage. The squares correspond to (1×1), c(2×2), and (2×2)-N/Fe(100) structures, the triangles represent (1×1) and $(\sqrt{3} \times \sqrt{3})$R30°-N/Fe(111) structures, and the circles represent (1×1) and (2×2)-N/(110) structures.

In Ref. (25), we suggest that the top layer of the Fe(111) surface reconstructs into islands of the c(2×2)-N/Fe(100) structure in order to gain the large extra binding energy in this structure. This can explain both the observed high binding energy and the large unit cell structures. If this is correct, it means that there are two kinds of adsorbed N on Fe(111): a simple overlayer structure on the unreconstructed surface with a fairly small binding energy, and a stronger bound island structure, which is locally (2×2)-N/Fe(100)-like. The resulting adsorption energy on the reconstructed Fe(111) surface will then be close to, but less negative than, that on the (100) surface as observed experimentally (15).

5.2. *Diffusion*

The diffusion of atomic nitrogen on the surface is an important part of the complete reaction. Figure 6 shows the calculated energy along the diffusion path.

In the equilibrium state, N is in a hollow site coordinating to a third layer Fe atom. Due to the symmetry of the surface, there are three equivalent sites in one unit cell. We find the barrier for going from one such site to another in the same hollow to be 0.71 eV, and the barrier for diffusing to another hollow to be 0.88 eV. The energy along the two paths were also found on an unrelaxed surface, where only the N atom was allowed to move. This gives the dashed lines in Fig. 6. The barriers on the static substrate are found to be smaller. This is because the ground state for the N atom is stabilized by 0.20 eV by allowing for surface relaxations while the two transition states are much less stabilized.

5.3. *Molecularly Adsorbed N_2*

The structures of the molecularly adsorbed states are shown in Fig. 7. Of the three possible perpendicular states coordinated to a single Fe atom, the one adsorbed on top of the first layer Fe atom is bound most strongly. This we identify as the γ state. In the experiment by Grunze *et al.* (17), a δ state was found. This state is less stable than the γ state and only populated when the surface is saturated with γ-N_2. The perpendicular state on top of the second layer Fe atom that we have found is less stable than the γ state by 0.14 eV and we will refer to this state as the δ state. The state coordinated to the Fe atom in the third layer is much less stable.

Two parallel states are found (shown to the right in Fig. 7). There is a symmetric configuration and an asymmetric configuration. According to Freund *et al.* (30) the α state adsorbs in an asymmetric coordination site, so we identify the asymmetric state in Fig. 7 with the α state. The symmetric state, which we call α', is a new state determined from our calculations.

Table 1 shows a number of characteristics for the γ, α, and α' states, comparing them with experiment where possible.

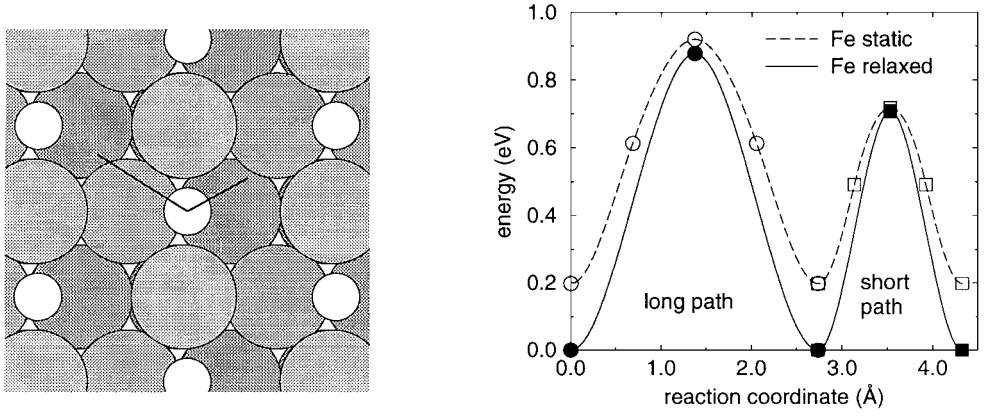

FIG. 6. Left: Diffusion of atomic N on the unreconstructed Fe(111) (1×1) surface. The lines show the possible jumps the N atoms can make. Right: Energy along the diffusion path. There are two inequivalent types of jumps: a short (squares) and a long (circles). Relaxations are included for both paths (full lines and filled symbols). The diffusion barriers have also been calculated on a static substrate (dashed line and open symbols). Energies are calculated using the PW91 exchange-correlation energy functional.

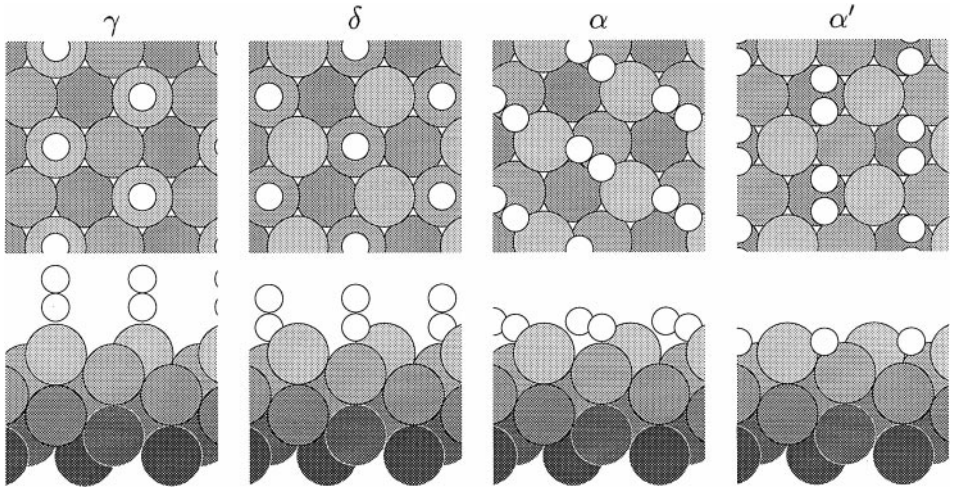

FIG. 7. Molecular states for N_2 on Fe(111). Top and side views are shown. There are two perpendicular states, γ and δ. Of the two parallel states there is an asymmetric and a symmetric state, α and α', respectively.

The calculated shifts in the vibrational frequency from the gas phase to the γ and α states are in good agreement with experiment; see Table 1. This supports our assignment of the two states. The N–N bond lengths and the N N frequencies shown in Table 1 give an indication of the strength of the N–N bond. A large d(N–N) and a small $\hbar\omega$ indicate a weak N–N bond. Comparing the numbers from the table, one would expect that the α' state is the best initial state for dissociation.

The calculated adsorption energies for 1 and 1/3 ML show that apparently there is no coverage dependence for γ while there is a strong coverage dependence for α and α'. This is because the parallel states bind to more than one Fe atom (31).

It is useful to compare the N/Fe(111) structure in Fig. 4 with the α'-N_2/Fe(111) structure in Fig. 7. In the α' state each of the two N atoms occupy almost identical sites to the single N atoms. In order to dissociate from the α' state, one atom will have to move into a neighboring hollow, leaving the other atom in the energetically most favorable state.

TABLE 1

Vibrational Frequencies for $^{15}N_2$, Frequency Shifts from the Gas-Phase Value, Adsorption Energies, and N–N Distance

x	γ	α	α'
$\hbar\omega$ (meV):	268(260)[a]	213(185)[b]	143
$\hbar\omega - \hbar\omega_{gas}$ (meV):	−21(−22)[a]	−76(−97)[b]	−146
E_x(1 ML) (eV/molecule):	−0.34	−0.15	−0.01
E_x(1/3 ML) (eV/molecule):	−0.35(−0.3)[c]	−0.41(−0.33)[d]	−0.17
d(N–N) (Å):	1.15	1.19	1.30

Note. Experimental numbers are given in parentheses when available.
[a] Ref. (20).
[b] Ref. (19).
[c] Ref. (17).
[d] Ref. (15).

The α' state has not been described before. It is less stable than the γ or the α states and will have a lifetime so short that direct experimental observation will be difficult. Yet, it is the most likely precursor to dissociation.

6. THE DISSOCIATION PROCESS

In this section we will discuss the dissociation process. We will consider the direct adsorption into each of the molecular states discussed above, and we will also consider transformations from one state to the next. For each of the elementary process we determine the minimum energy path. We have used the Ulitsky–Elber method discussed in Refs. (31, 32) to find minimum energy paths between the different molecular states as well as dissociation paths from molecular states to the atomic state. The energy along the path will be shown as a function of the reaction coordinate s, which is defined as $ds = |d\mathbf{R}|$ or, with discrete points, as $\Delta s = |\mathbf{R}_{i+1} - \mathbf{R}_i|$, where the vector $\mathbf{R}$ holds all six Cartesian N_2 coordinates. For all configurations on the paths we know the force $\mathbf{F}$ and the unit vector along the path $\mathbf{c}$. This gives us the slope $dE/ds = -\mathbf{c} \cdot \mathbf{F}$. The calculated slopes allow one to draw a smooth curve through each point. An example is given in Fig. 8.

6.1. Direct Adsorption

We have investigated the direct adsorption into (and desorption from) the four molecular states shown in Fig. 7. The energy as a function of the height of the molecule above the top Fe layer is shown in Fig. 9. The paths found correspond to minimum energy paths from the molecularly adsorbed states to molecules with the same orientation directly above the surface.

A molecule that approaches the surface with its axis perpendicular to the surface will be attracted toward the γ

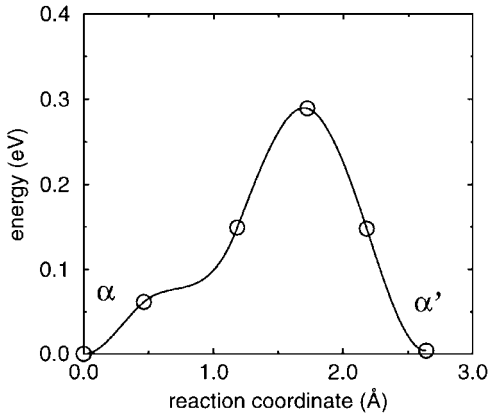

FIG. 8. The minimum energy path for the $\alpha \rightarrow \alpha'$ step using the Ulitsky–Elber method, and calculated in a (1×1) unit cell using PW91 energies and forces. The energy along the path is shown as a function of the reaction coordinate. The calculated slopes allow one to draw a smooth curve.

state. There is essentially no barrier for this adsorption. Adsorption directly into the δ state has a small barrier. There are also barriers for a molecule oriented parallel to the surface approaching the α and α' states. These results are in good agreement with experiment: At low temperatures, only the γ state has a sticking probability close to one.

6.2. *Indirect Adsorption*

Since the adsorption into the γ state is easy, we look for a path from this state to the dissociated state β (see Fig. 4). There are many possibilities for such a minimum energy path. We propose the following (see Fig. 11): $\gamma \rightarrow \delta \rightarrow \alpha \rightarrow \alpha' \rightarrow \beta$.

The transition state for the first step is shown in Fig. 10. The second step, also shown, is a rotation of the molecule taking place on top of a second layer Fe atom.

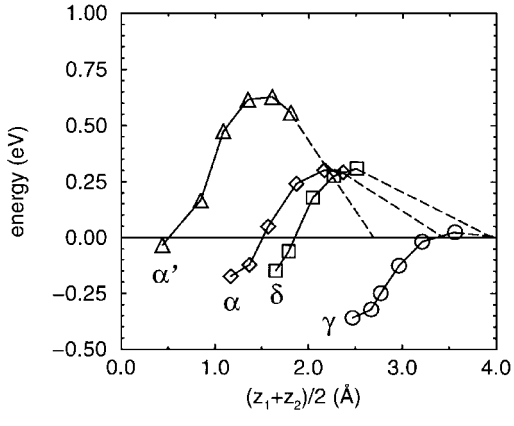

FIG. 9. Energy along paths perpendicular to the Fe(111) surface into the γ, δ, α, and α' states. $(z_1 + z_2)/2$ is the height of the N_2 center of mass above the top Fe layer. The separated molecule and slab defines the zero of energy. The dashed lines indicate that all curves will tend to zero far above the surface. The calculations are performed at a N_2 coverage of 1 ML.

From the α state the molecule makes a transition into the α' state and from the α' state it dissociates. We have not been able to find a path for dissociation directly from α to β with a lower barrier than for the indirect path via α'. The transition states for the paths from α to α' and further from α' to β are also included in Fig. 10. It is seen that from the transition state to the final state of the last step, the two N atoms bind to different Fe atoms. The alternative path where the N atom moves around the Fe atom which is coordinated to the other N atom has a considerably higher barrier. The fact that in the path shown in Fig. 10 no Fe atoms are shared between the two N atoms helps stabilize this part of the reaction (31).

The energy along the proposed path is shown in Fig. 11. The energy entering into the expression for the dissociation rate (Eq. [6].) should be corrected for zero point energies. We also show such an energy curve, $E^{\text{eff}}(s)$, in Fig. 11, where we have included the most important of the zero point energies coming from the N–N vibration. All other frequencies are much lower and will not be as important. It is clear that $E^{\text{eff}}(s)$ never gets much higher than zero, showing that the effective activation energy $E_{\text{TS}}^{\text{eff}}$ must be close to zero, as observed experimentally. Since all barriers are almost equal, the entropy of the transition states will also be important in determining which is the rate limiting step in the dissociation process. This suggests that one of the later steps is the slowest since the interaction with the surface is strongest and the transition state is most confined here. The two last steps, $\alpha \rightarrow \alpha'$ and $\alpha' \rightarrow \beta$, are both candidates. The DFT results indicate that the barrier is slightly larger for the last step, but the accuracy of the calculation is not good enough to distinguish, particularly since the two steps are of a very different character; $\alpha \rightarrow \alpha'$ is a molecular reorientation on the surface, whereas $\alpha' \rightarrow \beta$ involves the breaking of the N–N bond. Either way, the barrier is in excellent agreement with the experimental data for the adsorption of a thermal gas of N_2 above a Fe(111) surface. The maximum barrier we find is about $E_{\text{TS}}^{\text{eff}} = 0.1$ eV, close to the $E_{\text{TS}} = 0.03$ eV that we found above fitted the experimental data best. The difference between the two barriers is well below the accuracy of the calculation.

In the transition state theory estimate of the dissociation rate in Section 3 we assumed that the normal mode frequencies of the transition state complex were all high compared to kT, giving a partition function for the transition state for the dissociation step (q_{TS}) close to one. Around room temperature, $kT \sim 25$ meV, Eq. [7] shows that only frequencies below ~25 meV will result in a partition function substantially higher than one. We have made a normal mode analysis of the transition state of $\alpha \rightarrow \alpha'$ including only the six N_2 degrees of freedom. The frequencies are 193, 51, 36, 32, 25, and 23i meV. This analysis is very approximate because changes in the force constants for the Fe atoms have not been included, and the dynamical coupling between the

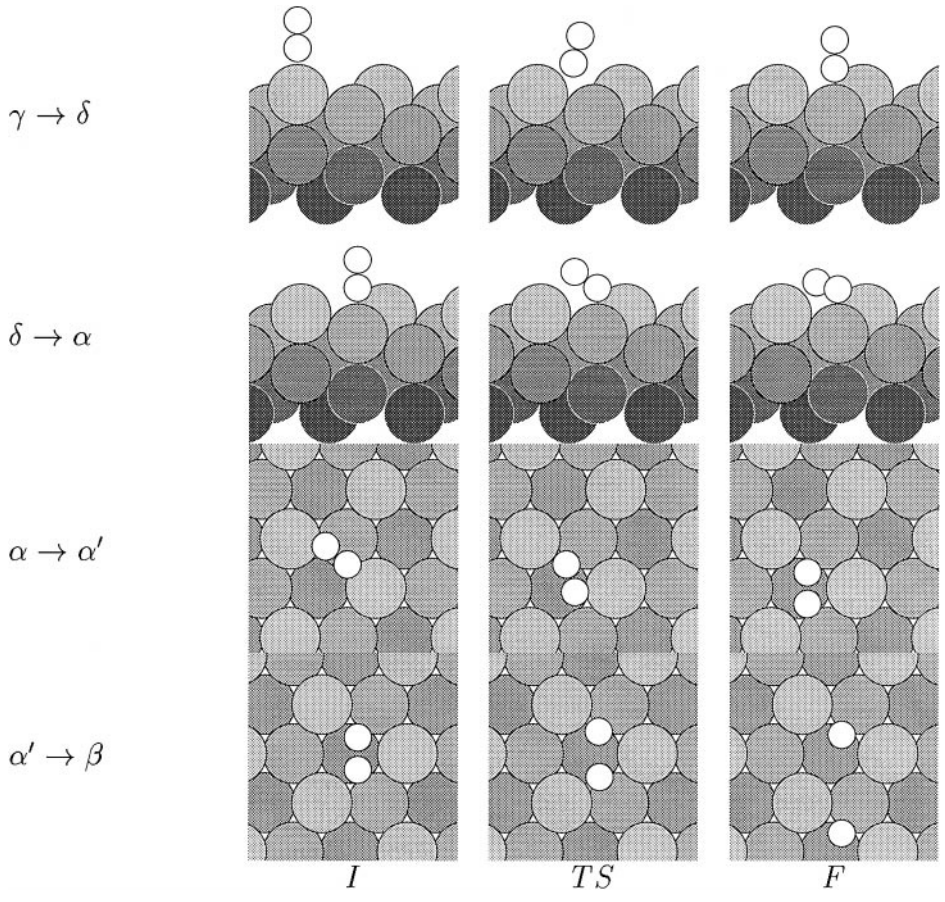

FIG. 10. Initial, transition, and final states for the N_2 transitions $\gamma \to \delta$ (side view), $\delta \to \alpha$ (side view), $\alpha \to \alpha'$ (top view), and $\alpha' \to \beta$ (top view) on Fe(111).

surface modes and the low energy N_2 modes can be substantial. Since a complete analysis is beyond present computational capabilities, we conclude that the assumption of $q_{TS} \sim 1$ is not unreasonable. We expect the same to be true for the $\alpha' \to \beta$ step, since the two N atoms are almost decoupled at the transition state and the N–Fe frequencies are large compared to room temperature. No matter whether $\alpha \to \alpha'$ or $\alpha' \to \beta$ (or both) is rate limiting, there is thus consistency between the calculated potential energy function $E^{\text{eff}}(s)$ in Fig. 11 and all experimental observations regarding the adsorption of a thermalized gas of N_2 over a Fe(111) surface as summarized in Fig. 2.

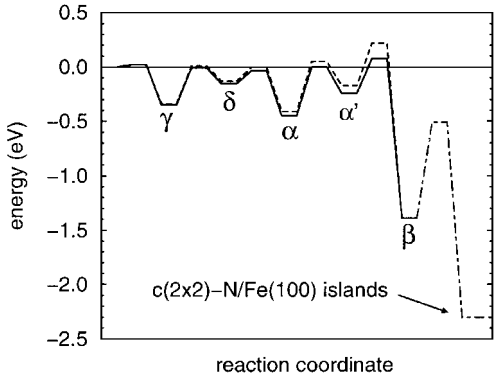

FIG. 11. Potential energy diagram for dissociative adsorption of N_2 on Fe(111). The zero of energy corresponds to the molecule in the gas phase. The dashed line shows the potential energy without correction for zero point energy, while the full line includes zero point energy for the N–N vibration. The dot-dashed line represents the transition from the simple N overlayer shown in Fig. 4 to N islands with a c(2 × 2)-N/Fe(100) structure.

We can write part of the prefactor in the expression for the sticking probability, σ_β, in Eq. [6] as

$$\frac{q_{TS}}{q_{gas}} = e^{-\Delta S/k}, \qquad [9]$$

and the small q_{TS}/q_{gas} leading to the small value for σ_β can therefore also be expressed as a large entropic barrier $\Delta S = S_{gas} - S_{TS}$.

The existence of the new α' state gives a new possibility for understanding the beam experiments by Rettner and Stein (14) provided we assume $\alpha \to \alpha'$ to be slightly slower than $\alpha' \to \beta$. With a beam of energy selected N_2 molecules, the beam energy determines which of the molecular states can be accessed directly; cf. Fig. 9. As the beam energy

increases, first the γ, then the δ, and then the α states can be accessed, and since the rate of reaching the β state increases along this series, the total sticking probability should increase. It will still be small, though, since the rate of going from any of these to the α' state is very low (or, to put it differently, the rate of desorption from any of these states is much larger than the rate of dissociation due to the entropic constraints of the $\alpha \rightarrow \alpha'$ transition state discussed above).

When the beam energy is high enough to give access directly into the α' state, on the other hand, the slow step from α to α' is bypassed. Once in the α' state, the rate of dissociation and the rate of conversion to α will be comparable, and much larger sticking probabilities will be possible. If the molecules equilibrate in the α' state, the surface temperature dependence of the sticking probability will be given by $e^{-\Delta E/kT}$, with $\Delta E = E_{\mathrm{TS}}^{\alpha' \rightarrow \beta} - E_{\mathrm{TS}}^{\alpha' \rightarrow \alpha}$. Both the calculation and experiment show that there should be such a temperature dependence and that it should be weak (ΔE is small).

We note that access into the α' state will probably not be associated with a large entropic barrier, since the transition state is far outside the surface (cf. Fig. 9), where the N_2 translations and rotations are not expected to be stiff.

6.3. *Promotion by Alkali Metals*

Adsorbed alkali metals promote both the N_2 adsorption process (8, 15, 20) and the ammonia synthesis reaction (34). It has been shown that the interactions between the adsorbed alkali atoms and the adsorbing N_2 molecule is dominated by the eletrostatic interaction between the two (35). The alkali atoms induce an electrostatic field $\mathcal{E}$ at the site of the N_2 molecule which has a dipole moment μ. The interaction is then

$$E_{\mathrm{dip}} = -\mathcal{E}\mu. \qquad [10]$$

We have calculated the dipole moments for the different adsorbed states and the $\alpha \rightarrow \alpha'$ transition state. The results are shown in Table 2. In this table we also include an estimate of the electrostatic interaction assuming that an alkali atoms (K) induces a field of the order 1 V/Å . This is a typical value as deduced from the work function change or calculated fields for alkalis outside Ru(0001) (35). The result is that both the α state and the transition state are stabilized by about 0.1 eV, in good agreement with experiment.

TABLE 2

Calculated Dipole Moments for N_2 in Different Sites on the Fe(111) Surface

	μ (eÅ)	E_{dip} (eV)
α:	−0.12	−0.12
$\alpha \rightarrow \alpha'$:	−0.09	−0.09
α':	−0.06	−0.06
$\alpha' \rightarrow \beta$	−0.11	−0.11

Note. Also included is the dipole interaction energy Eq. [10] assuming a field of 1 V/Å.

7. IMPLICATIONS FOR THE AMMONIA SYNTHESIS REACTION

The high barrier process directly into the α' state is much slower than the indirect process at low temperatures. We can estimate the dissociation rate of the direct process as

$$\sigma_\beta^{\mathrm{dir}} = s_0 \exp(-E^{\mathrm{dir}}/kT). \qquad [11]$$

If we use the calculated barrier of 0.64 eV (cf. Fig. 9) and a prefactor of $s_0 = 0.17$, the dissociation rate, shown as a dashed line in Fig. 2, follows. The prefactor is chosen as the high energy limit of the measured sticking probability in the molecular beam experiments (14). s_0 is not unity because only molecules impacting with the right orientation and position in the surface unit cell can stick (33) and only a certain fraction of those molecules entering into the α' state will dissociate at a given surface temperature.

It is clear from Fig. 2 that the indirect, low barrier process dominates for low temperatures including those normally used during industrial ammonia synthesis. Given the uncertainty of the estimate for $\sigma_\beta^{\mathrm{dir}}$ above, the possibility that the direct process can be important at the highest temperatures cannot be dismissed. The possibility that a direct process is important has been discussed earlier by Bowker (36) and Stoltze and Nørskov (37).

8. SUMMARY

In conclusion, we have made an extensive DFT study of the adsorption and dissociation of N_2 on Fe(111). We find all the experimentally observed states of N_2 on Fe(111) (α, β, γ, and δ), and can describe bond energies, structures, and vibrational frequencies in detail.

We have also found a new molecularly adsorbed state for N_2 (α'). This adds yet another potential energy well to the established picture of N_2 dissociation on Fe(111) (Fig. 1). The new state is the true precursor for dissociation. Instead of dissociating directly from the α state, the molecule must first enter the new precursor state before it can dissociate. A complicated dissociation path $\gamma \rightarrow \delta \rightarrow \alpha \rightarrow \alpha' \rightarrow \beta$ is suggested, which has essentially no barrier for dissociation, but a large entropic barrier due to the restricted transition state for the step $\alpha \rightarrow \alpha'$ and $\alpha' \rightarrow \beta$. We also identify a direct, activated path into the α' state. Here the entropic barrier is small, and this can give high sticking probabilities at high temperatures or in molecular beam scattering experiments.

Under normal ammonia synthesis conditions the low barrier, high entropy path will dominate, but at the highest temperatures, the high barrier process may become effective.

ACKNOWLEDGMENTS

Discussion with and inspiration from I. Alstrup, F. Besenbacher, M. Boudart, I. Chorkendorff, J. A. Dumesic, G. Ertl, M. V. Ganduglia-Pirovano, A. Nielsen, G. A. Somorjai, P. Stoltze, H. Topsøe, and E. Törnqvist are gratefully acknowledged.

The present work was in part financed by The Danish Research Councils through The Center for Surface Reactivity and Grant #9501775. The Center for Atomic-Scale Materials Physics is sponsored by the Danish National Research Foundation.

REFERENCES

1. Grunze, M., *in* "The Chemical Physics of Solid Surfaces and Heterogeneous Catalysis" (D. A. King and D. P. Woodruff, Eds.), Vol. 4, p. 143. Elsevier, New York, 1982.
2. Scholten, J. J. F., Zwietering, P., Konvalinka, J. A., and Boer, J. H., *Trans. Faraday Soc.* **55**, 2166 (1959).
3. Nielsen, A., "An Investigation on Promoted Iron Catalysts for Ammonia Synthesis." Jul. Gjellerups Forlag, 1968; *Catal. Rev.* **4**, 1 (1997).
4. Ozaki, A., and Aika, K., *in* "Catalysis: Science and Technology" (J. R. Anderson and M. Boudart, Eds.), Vol. 1. Springer Verlag, Berlin, 1981.
5. Dumesic, J. A., Topsøe, H., and Boudart, M., *J. Catal.* **37**, 513 (1975).
6. Ponec, V., and Knor, J., *J. Catal.* **10**, 73 (1968).
7. Ertl, G., *Catal. Rev. Sci. Eng.* **21**, 201 (1980).
8. Spencer, N. D., Schoonmaker, R. C., and Somorjai, G. A., *J. Catal.* **74**, 129 (1982).
9. Topsøe, H., Boudart, M., and Nørskov, J. K., Eds., "Frontiers in Catalysis: Ammonia Synthesis and Beyond," Topics in Catalysis, Vol. 1, p. 185. Baltzer, Basel, 1994.
10. Stoltze, P., and Nørskov, J. K., *Phys. Rev. Lett.* **55**, 2502 (1985); *J. Catal.* **110**, 1 (1988).
11. Bowker, M., Parker, I., and Waugh, K. C., *Surf. Sci.* **197**, L223 (1988).
12. Aparicio, L. M., and Dumesic, J. A., *in* "Frontiers in Catalysis: Ammonia Synthesis and Beyond" (H. Topsøe, M. Boudart, and J. K. Nørskov, Eds.), Topics in Catalysis, Vol. 1, p. 233. Baltzer, Basel, 1994.
13. Alstrup, I., Chorkendorff, I., and Ullmann, S., *Z. Phys. Chem.* **198**, 123 (1997).
14. Rettner, C. T., and Stein, H., *Phys. Rev. Lett.* **59**, 2768 (1987).
15. Bozso, F., Ertl, G., Grunze, M., and Weiss, M., *J. Catal.* **49**, 18 (1977); Ertl, G., Lee, S. B., and Weiss, M., *Surf. Sci.* **114**, 515 (1982).
16. Bozso, F., Ertl, G., Grunze, M., and Weiss, M., *J. Catal.* **50**, 519 (1977).
17. Grunze, M., Strasser, G., Golze, M., and Hirschwald, *Appl. Phys. A* **44**, 19 (1987).
18. Grunze, M., Golze, M., Fuhler, J., Neumann, M., and Schwarz, E., *in* "Proceedings, 8th International Congress on Catalysis, Berlin, 1984," Vol. 4, p. 133. Dechema, Frankfurt-am-Main, 1984.
19. Grunze, M., Golze, M., Hirschwald, W., Freund, H.-J., Plum, H., Seip, U., Tsai, M. C., Ertl, G., and Küppers, J., *Phys. Rev. Lett.* **53**, 850 (1984).
20. Whitman, L. J., Bartosch, C. E., Ho, W., Strasser, G., and Grunze, M., *Phys. Rev. Lett.* **56**, 1984 (1986).
21. Imbihl, R., Behm, R. J., Ertl, G., and Moritz, W., *Surf. Sci.* **123**, 129 (1982).
22. Atkins, P. W., "Physical Chemistry." Oxford Univ. Press, Oxford, 1990.
23. Kresse, G., and Furthmüller, J., *Comput. Mat. Sci.* **6**, 15 (1996).
24. Vanderbilt, D., *Phys. Rev. B* **41**, 7892 (1990).
25. Mortensen, J. J., Ganduglia-Pirovano, M. V., Hansen, L. B., Hammer, B., Stoltze, P., and Nørskov, J. K., *Surf. Sci.*, in press.
26. Perdew, J. P., Chevary, J. A., Vosko, S. H., Jackson, K. A., Pederson, M. R., Singh, D. J., and Fiolhais, C., *Phys. Rev. B* **46**, 6671 (1992).
27. Perdew, J. P., Burke, K., and Ernzerhof, M., *Phys. Rev. Lett.* **77**, 3865 (1996).
28. Zhang, Y., and Yang, W., *Phys. Rev. Lett.* **80**, 890 (1998).
29. Hammer, B., Hansen, L. B., and Nørskov, J. K., to be published.
30. Freund, H.-J., Bartos, B., Messmer, R. P., Grunze, M., Kuhlenbeck, H., and Neumann, M., *Surf. Sci.* **185**, 187 (1987).
31. Mortensen, J. J., Morikawa, Y., Hammer, B., and Nørskov, J. K., *J. Catal.* **169**, 85 (1997).
32. Ulitsky, A., and Elber, R., *J. Chem. Phys.* **92**, 1510 (1990). In the formulation we use the method is a simplified version of the method of Mills, G., Jónsson, H., and Schenter, G. K., *Surf. Sci.* **324**, 305 (1995).
33. Karikorpi, M., Holloway, S., Henriksen, N., and Nørskov, J. K., *Surf. Sci.* **179**, 241 (1987).
34. Törnqvist, E., and Chen, A. A., *Catal. Lett.* **8**, 359 (1991).
35. Nørskov, J. K., Holloway, S., and Lang, N. D., *Surf. Sci.* **137**, 65 (1984); Nørskov, J. K., *in* "The Chemical Physics of Solid Surfaces and Heterogeneous Catalysis" (D. A. King and P. Woodruff, Eds.), Vol. 6, Chap. 1. Elsevier, Amsterdam, 1993; Mortensen, J., Hammer, B., and Nørskov, J. K., *Phys. Rev. Lett.* **80**, 4333 (1998).
36. Bowker, M., *in* "Frontiers in Catalysis: Ammonia Synthesis and Beyond" (H. Topsøe, M. Boudart, and J. K. Nørskov, Eds.), Topics in Catalysis, Vol. 1, p. 265. Baltzer, Basel, 1994.
37. Stoltze, P., and Nørskov, J. K., *in* "Frontiers in Catalysis: Ammonia Synthesis and Beyond" (H. Topsøe, M. Boudart, and J. K. Nørskov, Eds.), Topics in Catalysis, Vol. 1, p. 253. Baltzer, Basel, 1994.